Spatiotemporal oscillations in a semiconductor étalon

Yu. A. Rzhanov and H. Richardson
Department of Physics, Heriot-Watt University, Riccarton, Edinburgh EH14 4AS, Scotland

A. A. Hagberg and J. V. Moloney
Department of Mathematics, University of Arizona, Tucson, Arizona 85721
(Received 16 July 1992)

We show theoretically that competing optical nonlinearities in a semiconductor étalon, with transverse effects included, result in complex spatiotemporal behavior. A theoretical framework is developed that explains many features of the oscillatory behavior. Numerical simulations exhibit kinks, switching waves, whole-beam, and edge oscillations. Simulations compare favorably with recent experiments.

PACS number(s): 42.65.−k

I. INTRODUCTION

Coupled nonlinear reaction-diffusion systems offer much scope for complex spatiotemporal behavior. One such system is the semiconductor Fabry-Pérot étalon having a refractive index dependent on photoexcited carrier density and temperature. These devices have attracted much interest due to potential applications to the fields of telecommunications and optical computing. Recent experiments in InSb devices have revealed complex oscillatory behavior of a reflected beam [1], posing intriguing questions about the nature and form of the oscillations. Furthermore, there has been no direct experimental evidence of transverse effects in the coupled InSb system, although these must play a crucial role in the dynamics of oscillations. To date theoretical considerations have concentrated on plane-wave approaches, which do not include spatial effects and hence are inadequate in describing oscillatory behavior.

We propose a theoretical technique that is useful in explaining features of spatiotemporal behavior in certain reaction-diffusion systems. We believe that this technique is quite general and can be applied to explore different processes in two-component reaction-diffusion systems. Here we apply this technique to the model of an InSb interferometer with competing nonlinearities. In such a two-component system there are three important length scales: namely, the two characteristic diffusion lengths and the minimum modulation length of the inhomogeneous parameters. The technique requires that one diffusion length be much smaller than the other diffusion length and the modulation length of the inhomogeneous parameters. Then at any instant and for each spatial point it is possible to treat the other component and the inhomogeneous parameters as fixed parameters of the equation with the smallest diffusion length. If in addition the characteristic decay time of the variable with the shortest diffusion length is much smaller than the other decay time, then a further simplification occurs. Then the dynamics of the fast variable can be considered independently of the slow variables, as these do not have time to respond to changes in the fast variable. It is then possible to predict local dynamic behavior from a known state of the complete system. These conditions are met in the InSb system if the spot size of the incident beam is large compared to the carrier diffusion length.

We apply the technique and gain useful insight into features of the oscillatory behavior and particularly concentrate on transverse effects. We simulate the system numerically in one transverse direction and show how kink solutions, whole-beam oscillations, and pulse effects evolve. Furthermore, we find that the edges of the carrier profile may lose stability and oscillate at a much higher frequency than expected, considering the thermal relaxation time of the system.

The paper is organized as follows. The InSb Fabry-Pérot system is introduced and the model explained. We review previous results on kink solutions and regenerative oscillations that are essential for the understanding of the graphical technique. This technique is then explained using examples from numerical solution of the full dynamical system. Finally we consider the response to pulse inputs ("single-shot regime") and edge oscillations.

II. MODEL EQUATIONS FOR THE FABRY-PÉROT RESONATOR

In this section we introduce the equations (proposed in [2]) which we will use to describe the processes in a nonlinear Fabry-Pérot resonator. The InSb étalon is mounted on a heat sink and illuminated by a laser beam of wavelength λ. The optical properties of the étalon are governed by the dependence of the refractive index on photoexcited carrier density (N) and temperature (T) through

$$n(N,T) = n_0(T_\sigma) - \sigma_N N + \sigma_T(T - T_\sigma), \tag{1}$$

where σ_N and σ_T are positive constants. Since the radia-

tion is not significantly absorbed in the cavity we assume that it is possible to average N over the length of the cavity. Then neglecting diffraction and restricting diffusion to one transverse direction we obtain the following reaction-diffusion system for the photoexcited carrier density and temperature:

$$\frac{\partial N}{\partial t} = \frac{\alpha I_c(N,T,x)}{\hbar\omega} - \frac{N}{\tau_N} + D\frac{\partial^2 N}{\partial x^2}, \tag{2a}$$

$$\frac{\partial T}{\partial t} = \frac{Q(N,T,x)}{c\rho} - \frac{T-T_0}{\tau_T} + \kappa\frac{\partial^2 T}{\partial x^2}, \tag{2b}$$

where

$$I_c(N,T,x) = \frac{(1-e^{-\alpha l})(1+R_b e^{-\alpha l})(1-R_f)}{\alpha l(1-R_\alpha)^2} \times \frac{I_{\rm in}(x)}{1+F\sin^2[2\pi n(N,T)l/\lambda]} \tag{3}$$

is the cavity irradiance. The étalon is of length l and mirror reflectivities R_f (front), and R_b (back). The finesse factor $F = 4R_\alpha(1-R_\alpha)^{-2}$, where $R_\alpha = (R_f R_b)^{1/2}e^{-\alpha l}$. The intensity absorption coefficient may depend on temperature through

$$\alpha(T) = \alpha_0 \exp\left(\frac{T-T_\alpha}{\Theta}\right). \tag{4}$$

Both carriers and heat diffuse in the x direction with diffusion coefficients D and κ, respectively. τ_N is the carrier recombination time and is independent of N since we assume trap recombination as the dominant recombination mechanism (at $T_0 \approx 77$ K). $Q(N,T)$ represents the heat generated per unit volume and may be from two sources. First there is nonradiative carrier recombination, which yields

$$Q(N,T) = \hbar\omega\frac{N}{\tau_N}. \tag{5}$$

[Note that Eqs. (1)–(5) are in the form proposed in [2].] Second there could be absorption of radiation at the back mirror since some experiments utilize a gold reflecting layer to provide extra reflectivity. We could then assume a contribution of the form

$$Q(N,T) \approx \frac{\alpha_{\rm eff} I_t(N,T)}{\rho C l}, \tag{6}$$

where I_t is the "transmitted" irradiance and $\alpha_{\rm eff}$ takes account of any heating outside the étalon. This form of heat source has been shown to lead to oscillatory behavior in the plane-wave limit [3].

In Eq. (2b), we neglected the dependence of the lattice temperature on the coordinate z along the beam direction. This is an acceptable approximation if the InSb layer is in contact with a perfect heat sink through a thin thermal resistance [4], as is indeed the case experimentally. Then we may replace the term describing thermal diffusion in z ($\kappa\,\partial^2 T/\partial z^2$) with the decay term $-(T-T_0)/\tau_T$ used in (2b). τ_T plays the role of a thermal relaxation time and defines a corresponding diffusion length $l_T = \sqrt{\kappa\tau_T}$. This approximation leads to the following consequences:

TABLE I. Experimental parameters.

Quantity	Value or range	Units
T_0	77–85	K
T_σ, T_α	77	K
σ_N	1.6–5.0×10^{-18}	$\rm cm^3$
σ_T	6×10^{-4}	$\rm K^{-1}$
τ_N	300–600	ns
τ_T	70–500	ms
λ	5.43–5.71	μm
l	100–500	μm
R_f	0.36–0.5	
R_b	0.36–0.95	
α_0	2–80	$\rm cm^{-1}$
$\alpha_{\rm eff}$	0–1	
D	10	$\rm cm^2/s$
κ	0.01–0.1	$\rm cm^2/s$
C	0.096	J/g K
ρ	5.8	$\rm g/cm^3$
w	200	μm
θ	0–30	K

(i) Absorption at the back mirror must be treated as a heat source averaged over the cavity. This is a reasonable assumption if the length of the étalon is short compared to the characteristic thermal length.

(ii) Carrier recombination at the surfaces of the InSb is neglected. This effect could be included by adding a factor multiplying the incident irradiance in (2a) [5, 6].

As we intend to concentrate on transverse processes the precise forms of the source and sink terms are not important, as this is unlikely to affect the qualitative behavior of the system as a whole.

Even with the approximations noted above, this system is still too complex to treat analytically and also difficult to simulate numerically because of the large ratio of reaction rates ($\tau_T/\tau_N \sim 10^3$). In the following sections any numerical simulations are of the full system (2a) and (2b) assuming heating due to (bulk) carrier recombination only. References to a Gaussian input assume the profile

$$I_{\rm in}(x) = I_0 \exp(-x^2/w^2), \tag{7}$$

where I_0 is the peak irradiance and w the spot size. Typical experimental parameters are tabulated in Table I and we will use these parameters throughout. In the experiments performed to date there are many parameters that are not known precisely. In particular, the heat sources have not been quantified. Therefore we do not attempt *quantitative* agreement with experiments. We assume that the system will behave similarly in two transverse dimensions although the effective diffusion rate will be different.

III. THEORETICAL AND NUMERICAL TREATMENT

Before considering the complex spatiotemporal behavior of the InSb system we will present some previous re-

sults. Having presented the theoretical framework required we will build upon this to propose a technique for explaining the complex behavior of the system.

We begin by considering the one-component bistable system, which evolves according to

$$u_t = f(u, \boldsymbol{\lambda}), \tag{8}$$

where f depends on both u and the set of parameters $\boldsymbol{\lambda}$. There may be any number of roots of (8) satisfying the steady-state condition

$$f(u, \boldsymbol{\lambda}) = 0. \tag{9}$$

A common realization of f is the S shaped curve obtained by plotting the solution of Eq. (9) against one of the parameters (λ_1, say). An example is given in Fig. 1(a) where the system is bistable in the range $\lambda_1^a < \lambda_1 < \lambda_1^b$. λ_1 is typically an external parameter — for example, the incident irradiance in an optically bistable system. In the bistable region the state depends on previous history (this leads to the well-known hysteresis effect [7]). This property may be used to provide memory functionality in a single device. Another feature of these systems is that near the critical points $(\lambda_1^a, \lambda_1^b)$ there is very slow response. This is known as *critical slowing down* and is a limitation in marginal switching situations. In two-component systems this is not such an important effect. Inclusion of diffusion gives the equation

$$u_t = f(u, \boldsymbol{\lambda}) + D_u \frac{\partial^2 u}{\partial x^2}, \tag{10}$$

where D_u is the diffusion coefficient of the species u. Equation (10) has a nonhomogeneous solution even if $\boldsymbol{\lambda}$ and D_u are homogeneous. This separatrix solution has the following properties:

$$\lim_{x \to +\infty} u = u^+, \qquad \lim_{x \to -\infty} u = u^-,$$

$$\left.\frac{\partial u}{\partial x}\right|_{x=-\infty} = \left.\frac{\partial u}{\partial x}\right|_{x=+\infty} = 0,$$

where u^- and u^+ are the two stable zeroes of (9) corresponding to $\boldsymbol{\lambda}$ in the bistable region [Fig. 1(a)]. The two states are joined by a region of approximate width $\sqrt{D_u}$ as shown in Fig. 1(b). This *kink* solution is independent of transverse coordinate and hence will move with constant velocity. Assuming a solution of the form $u(x - Vt) \equiv u(\zeta)$ yields

$$V = -\frac{\int_{u^-}^{u^+} f(u', \boldsymbol{\lambda}) du'}{\int_{-\infty}^{+\infty} \left(\frac{du}{d\zeta}\right)^2 d\zeta}. \tag{11}$$

Of particular interest is the case when the kink is stationary, which requires

$$\int_{u^-}^{u^+} f(u', \boldsymbol{\lambda}) du' = 0. \tag{12}$$

For simple forms of f the velocity can be found analytically but in general numerical methods have to be used. Another approach is to recast (8) in the form typical of a system moving in a conservative field:

$$u_t = -\frac{dU}{du}, \tag{13}$$

where

$$U(u) = -\int f(u, \boldsymbol{\lambda}) du \tag{14}$$

is the potential. The velocity is then a function of the difference in potentials — the system moves to the most favorable state (lowest potential). When the potentials of the two states are equal the kink is stationary.

One-dimensional systems have been studied theoretically and experimentally using the above approaches (see, for example, references in Fife [7].) Harding and Ross [8] have experimentally investigated the dynamics of kink solutions in a ZnSe system with a thermal nonlinearity.

The next step in complexity is to consider a coupled reaction system:

$$\begin{aligned} u_t &= f(u, v, \boldsymbol{\lambda}), \\ v_t &= g(u, v, \boldsymbol{\lambda}). \end{aligned} \tag{15}$$

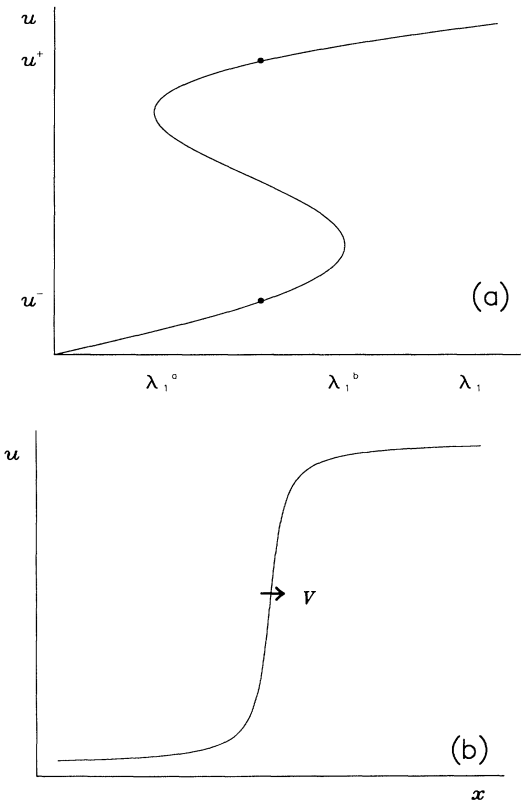

FIG. 1. (a) An S-shaped curve for $g(u, \lambda) = 0$ showing bistability in the range $\lambda_1^a < \lambda_1 < \lambda_1^b$. Two states are indicated within the bistable region. (b) Spatial kink solution between the two states depicted in (a).

The state of the system evolves in the phase space (u, v) and a convenient approach is the use of nullcline diagrams. The nullclines

$$f(u, v, \boldsymbol{\lambda}) = 0 \quad \text{and} \quad g(u, v, \boldsymbol{\lambda}) = 0$$

may be plotted in the u, v plane and an example is shown in Fig. 2, which shows one f and two g corresponding to different parameters. Intersections of the f and g nullclines correspond to steady-state solutions of *both* subsystems and hence of the complete system (15). In the example shown the system is in the bistable regime for the solid g nullcline and there are three steady-state solutions, two stable and one unstable. Local evolution of a state can be inferred in the following way. On each side of the curves $f = 0$ and $g = 0$ the sign of the derivatives du/dt and dv/dt changes. Hence u and v will increase or decrease depending on where the current state of the system is in relation to the nullclines. In some parameter regions there may be no stable states and this is indeed the case for the dotted g nullcline in Fig. 2, the result being that the system oscillates. In general the path in phase space is not easy to predict [9]. However, when one subsystem reacts much faster than the other (as in the InSb interferometer), the system will trace a path close to the N nullcline under the influence of any (slow) changes in T. In some parameter ranges a reduction in the slow variable may pull the state off the N nullcline and it will jump very quickly to the next available N state. An example is shown in Fig. 3, where there is fast initial movement from S to the N-nullcline. This is followed by a slow reduction in temperature until at point A the stability is lost causing a jump to state B, which occurs in a time of the order of the carrier relaxation time. Point B is below the T nullcline and hence the temperature will slowly rise and the state follows the N nullcline towards point C. At point C there is a jump to point D and the process repeats. These regenerative oscillations have been proposed [10] and studied theoretically and experimentally [11, 12] in optically bistable semiconductor systems. In most cases the plane-wave (homogeneous) description is used and in some cases the fast subsystem

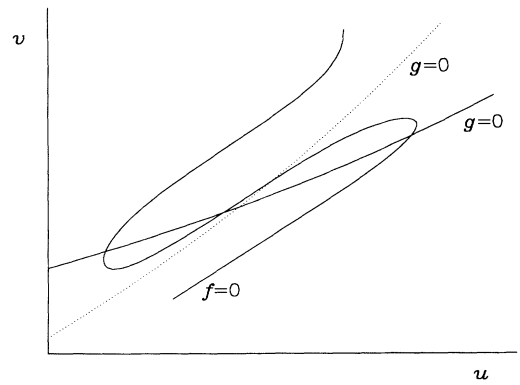

FIG. 2. The nullclines $f(u, v, \lambda) = 0$ and $g(u, v, \lambda) = 0$. For the solid g nullcline there are two stable and one unstable state. For the dotted g nullcline the stationary state is unstable and the system oscillates.

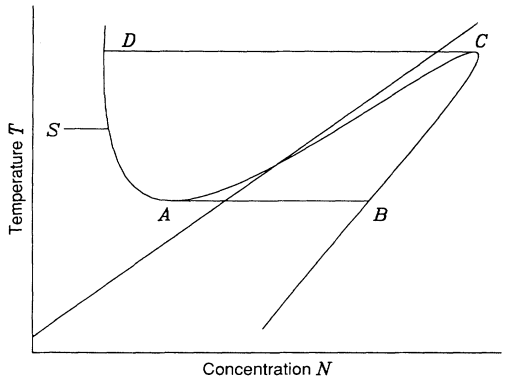

FIG. 3. The result of a numerical simulation overlayed on the nullcline figure. From the initial point S the system settles into an oscillatory motion.

is eliminated adiabatically. This is appropriate as long as the transverse effects may be neglected.

Now consider a two-component homogeneous reaction-diffusion system:

$$u_t = f(u, v, \boldsymbol{\lambda}) + D_u \frac{\partial^2 u}{\partial x^2},$$
$$v_t = g(u, v, \boldsymbol{\lambda}) + D_v \frac{\partial^2 v}{\partial x^2}. \tag{16}$$

In the bistable region the nullclines can be as shown in Fig. 4(a). As before—for a kink solution—we assume a state $A = (N_a, T_a)$ at $x = -\infty$ and $B = (N_b, T_b)$ at $x = +\infty$. It has been shown that either one or three traveling-wave solutions exist, depending on the ratio of characteristic velocities of the two subsystems [13, 14]. In a system with a large difference in reaction rates it is possible to decouple the equations and assume that the kink in the fast variable is only under the influence of the (local) state of the slow variable. To show this, a numerical simulation of the InSb system was performed with parameters corresponding to Fig. 4(a). The input intensity was constant in time and space and the initial profile set to $(N, T) = (N_a, T_a)$ for $x < 50 l_N$ and $(N, T) = (N_b, T_b)$ for $x > 50 l_N$. The results are shown in Fig. 4(b) where each carrier profile is separated by $\Delta t = 10 \tau_N$. Note that a kink forms between the values N_a and N_c. This moves rapidly and is almost unaffected by the very small change in temperature. On a much longer time scale the temperature decreases $(x > 50 l_N)$ and N reduces accordingly, following the nullcline from C to A. The important consequence is that the N kink can be considered as a one-component solution between N_b and N_c (or N_c and N_a), treating the temperature as a fixed parameter. Experiments are underway to examine these effects, although no convincing results have appeared.

Finally we consider the analysis of Nishiura and Mimura [15], who investigated a homogeneous reaction-diffusion system recast into the form

$$\varepsilon\tau u_t = f(u,v) + \varepsilon^2 \frac{\partial^2 u}{\partial x^2},$$
$$v_t = g(u,v) + \frac{\partial^2 v}{\partial x^2}, \tag{17}$$

under the assumption that u reacts much faster but diffuses to a lesser extent than v. Nontrivial layer solutions are possible in such a system for sufficiently small τ [16]. As τ is reduced further, the system may undergo a Hopf bifurcation and the edges of the layers become unstable and oscillate. The amplitude of oscillation increases as τ is reduced further. The bifurcation parameter is the ratio of characteristic velocities of the two subsystems:

$$\tau = \frac{V_v}{V_u} = \frac{l_v/\tau_v}{l_u/\tau_u}, \tag{18}$$

where l and τ are characteristic diffusion lengths and relaxation times, respectively. This parameter has been linked to the appearance of multiple moving structures in coupled reaction-diffusion systems [17] and later the link was proved numerically and by the singular perturbation approach [13]. Note also that as suggested by Kalafati, Serbinov, and Ryabova [17] τ also controls the number of traveling-wave solutions. For large τ [$O(1)$] there is only one solution and as τ is reduced, the system bifurcates and exhibits at least three solutions, one being unstable [14].

We have now considered the relevant effects that have been predicted or observed in *homogeneous* systems and will extend to consider an inhomogeneous system—the InSb system illuminated by a Gaussian beam. This will modify the behavior and in particular will limit the extent of any kink or layer solutions.

A. Whole-beam oscillations

Oscillations in the reflected power from an InSb bistable étalon have been observed experimentally [18] and described theoretically using a plane-wave approach [11]. Unfortunately there has been no direct measurement of the transverse dynamics of the oscillations. As a first attempt at describing the oscillations for a Gaussian input in one transverse coordinate we can consider the nullcline curves that predict behavior in the plane wave (Fig. 5). The path superimposed on the figure corresponds to the center of the beam and was obtained numerically. However, we find that the plane-wave approach does not give any valuable information about the behavior of the extended system. Indeed, when the plane-wave system has an oscillatory solution, the oscillations for a Gaussian beam with sufficiently small spot size are prevented by thermal diffusion in the transverse direction. Similarly, when the plane-wave approach predicts monostability (or bistability), the one-dimensional system may oscillate, as we will see later.

Now we will formulate a technique that takes into consideration the change in the spatial properties of the sys-

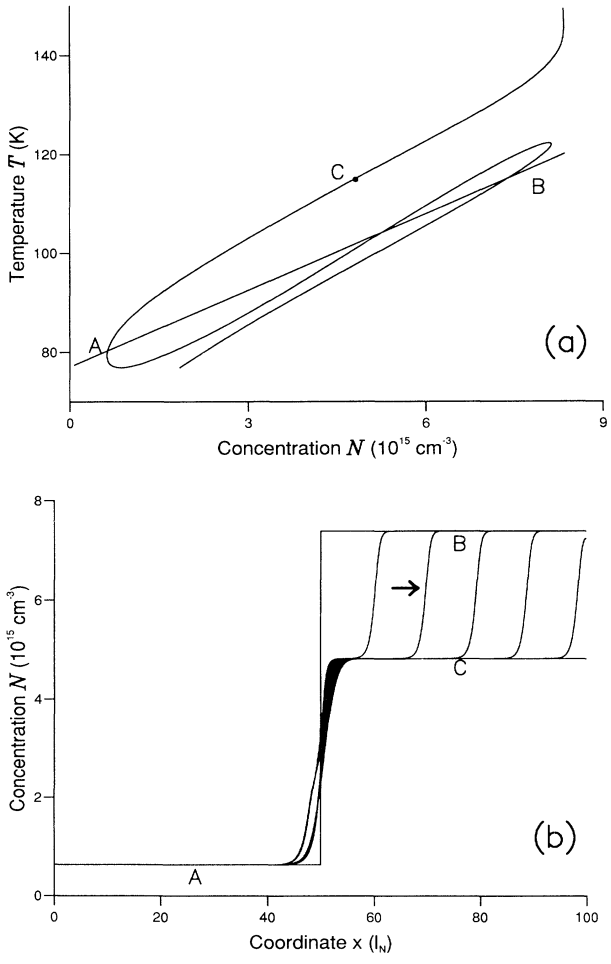

FIG. 4. (a) Nullclines showing the position of the states defining the kink solutions in (b). (b) Evolution of carrier density as a function of time showing development of kink solution. Each curve is separated by $\Delta t = 10\tau_N$.

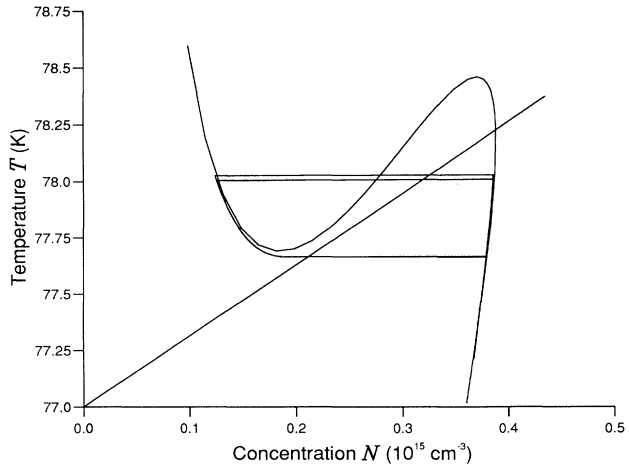

FIG. 5. An example of an oscillation in a Gaussian beam where the state in the center of the beam is plotted in phase space along with the nullclines. Note that the nullcline approach predicts the existence of one stable state.

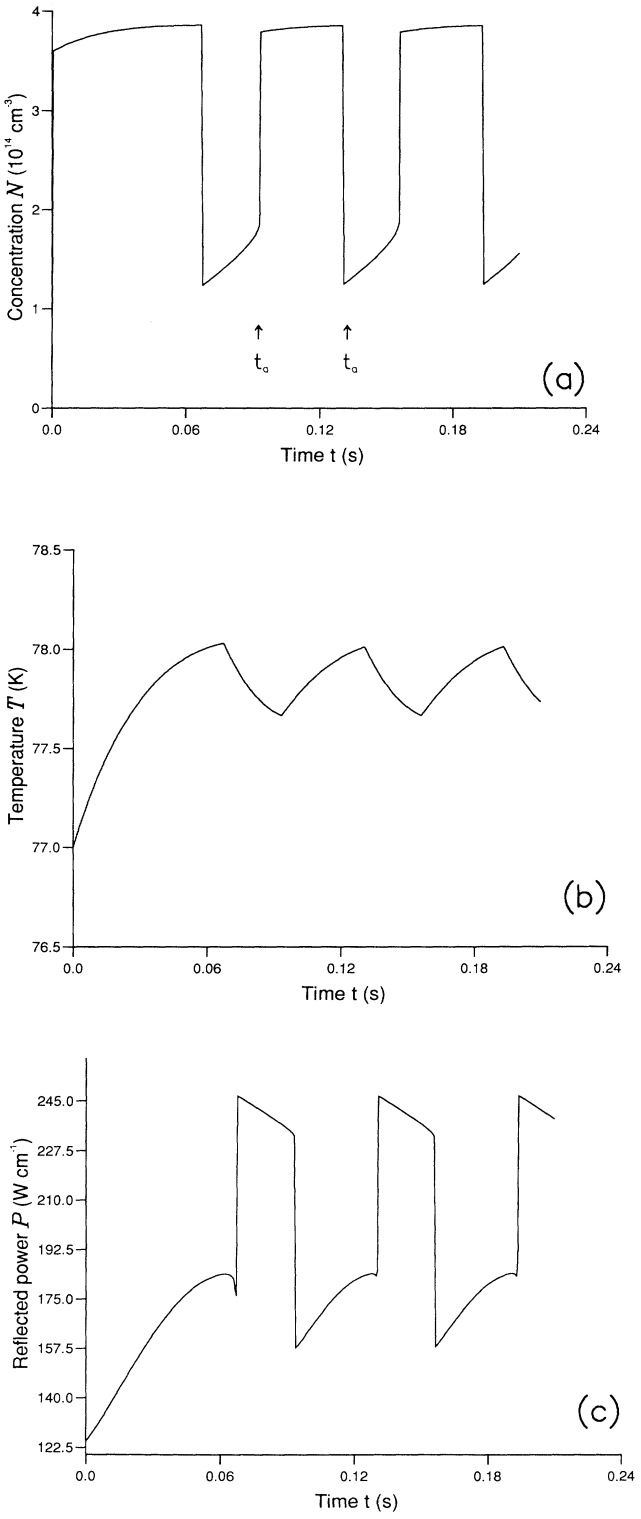

FIG. 6. Evolution of (a) central carrier density, (b) temperature (at the beam center), and (c) reflected power showing whole-beam oscillations. Parameters: $\lambda = 5.618$ μm, $D = 10$ cm^2/s, $\kappa = 0.01$ cm^2/s, $R_f = R_b = 0.5$, detuning=1.451 42, $T_0 = 77$ K, $\sigma_N = 1\times10^{-17}$ cm^{-3}, $\sigma_T = 6\times10^{-4}$ cm^{-3}, $\tau_N = 0.6$ μs, $\tau_T = 30$ ms, $\alpha_0 = 2.4$ cm^{-1}, $\theta = 30$ K, $I_0 = 3.5$ W/cm^2, $w = 60l_N$.

tem (intensity of the beam) and allows an adequate description of the oscillation process in an inhomogeneous medium.

First consider the features of the whole-beam oscillations found numerically. In Fig. 6 the evolution of central N, T and reflected power is shown and oscillations are evident. Figure 7(a) is a contour plot of carrier density as a function of x and time. Similarly, Fig. 7(b) shows the evolution of the temperature. As the time $t = t_a$ is approached the system is in the "lower" N state and is cooling. At $t = t_a$ the center of the carrier profile switches to the upper state and the switched-up region rapidly expands. The carrier profiles around the switch-up point are shown in Fig. 8(a), where each profile is separated by a time of $41.67\tau_N$. During the switch process the temperature changes by less than 0.01%. The region of high carrier density adds extra heat due to carrier recombination and hence the temperature rises. As the temperature increases the switched-up region contracts until it finally collapses at $t = t_b$ [Fig. 8(b)]. After collapse the

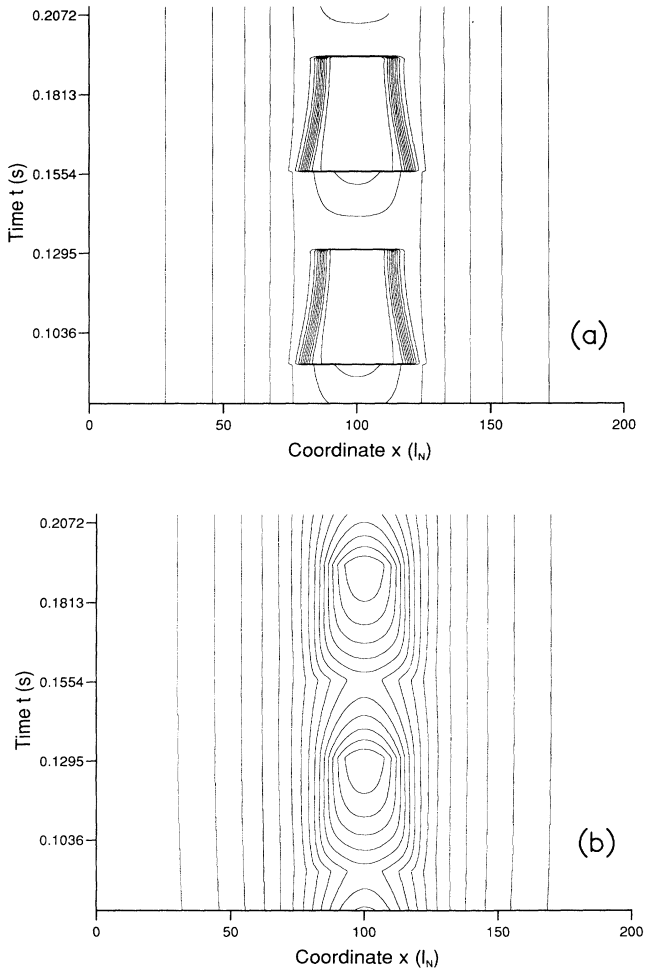

FIG. 7. Contour plot of (a) carrier density and (b) temperature as a function of position and time showing whole-beam oscillations.

heat source is reduced, the temperature decreases, and the whole process repeats.

B. *I-T* representation

It has already been demonstrated that because of the disparity in the time constants of the InSb system it is possible to neglect temporal variations in temperature while fast transverse motion of carrier density occurs. In addition to this the thermal length is much greater than both the likely variations in $N(x)$ and the spot size w. This allows us to consider kinks in carrier density as "homogeneous" ones. We therefore treat the N subsystem independently and may consider the local temperature as a fixed parameter. For any point (x_0, say) on the beam we can draw the N nullcline as shown in Fig. 9. If the temperature at x_0 is known, then in the vicinity of x_0 we can see if the system is stable or bistable in N. For $T > T_u$ and $T < T_l$ there is only one stable state. For $T_l < T < T_u$ the system is bistable and the state depends on the history or any spatial effects. In Fig. 10(a), T_l and T_u are graphed against the *intensity* $[I(x_0) = I_0 \exp(-x_0^2/w^2)]$. Choosing another point on the beam (x_1) yields a new T_l and T_u, and these may be plotted on the same diagram at the new intensity $I(x_1)$. Extending to all points on the beam yields the

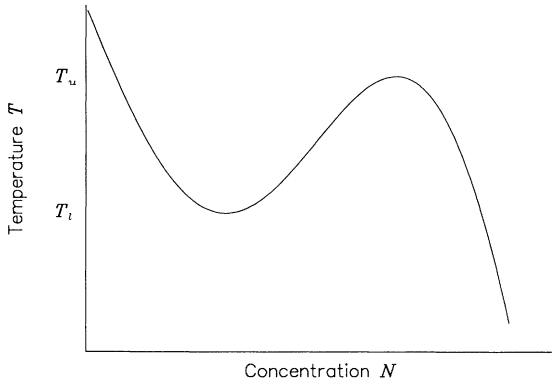

FIG. 9. N nullcline corresponding to one particular point in a beam. If the temperature lies between T_l and T_u, then the system is bistable in N. Outside this range only one state is possible.

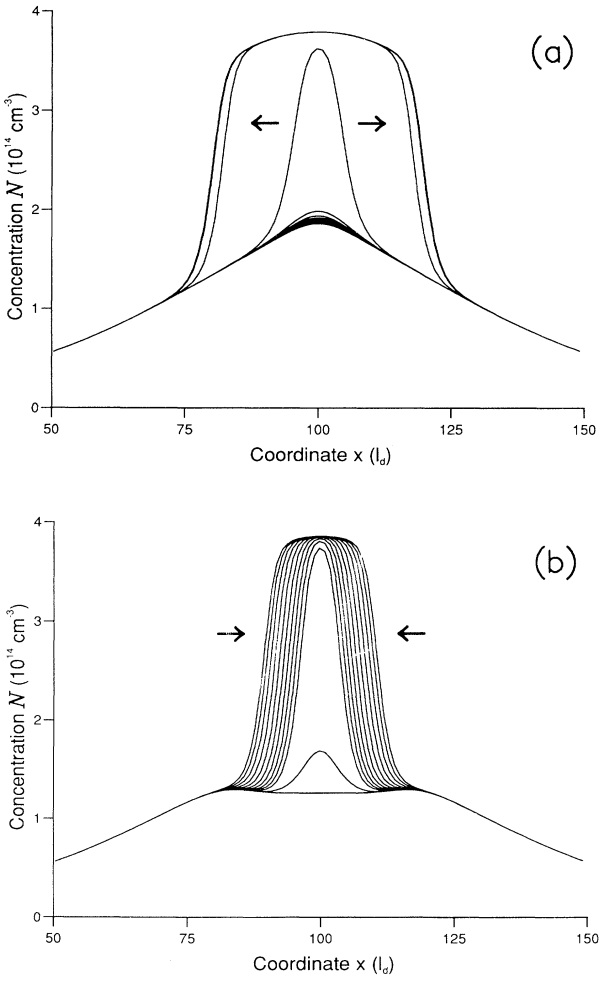

FIG. 8. Profiles of carrier density variation with x showing the (a) switch-on and (b) switch-off section of whole-beam oscillations. Each curve is separated by $\Delta t = 41.67\tau_N$.

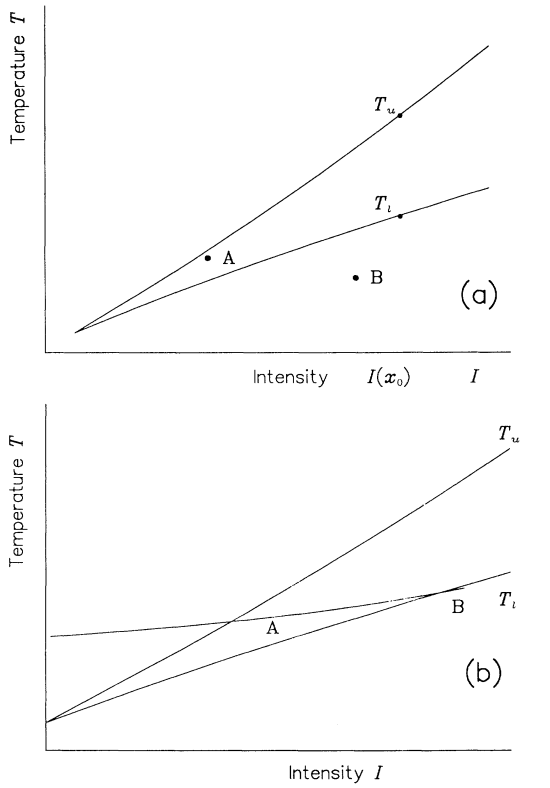

FIG. 10. (a) From an initial point (x_0) on the beam, T_l and T_u define the region of bistability. Extending to all spatial points yields the solid curves. (b) The beam curve through A and B passes through the bistable region bounded by the curves T_l and T_u.

solid curves which bound the region of bistability. Note that the diagram indicates *stability in N* as a function of local intensity and temperature under the assumptions made above. For all points below the lower curve (like B) there is only one possible state—the upper N state. For points inside the bistable region (like A) the system is bistable and hence either N state is possible. (Note that we are defining the state at each point in terms of slowly varying T and I and hence N is only allowed to take upper or lower bistable values. Of course these values depend on the local temperature and intensity.) Any particular solution may be plotted on the I-T diagram since the temperature at each spatial point is related to the irradiance through the coordinate x. We will refer to this curve as the *beam curve* in further discussions. If $x \in [x_a, x_b]$, then for a Gaussian input the beam curve starts at $(I(x_a), T(x_a))$, reaches $I = I_0$, and ends at $(I(x_b), T(x_b))$.

In Fig. 10(b) the curve $T(I(x))$ has been added, which represents a solution where at point B the upper N state is realized. The system is in the lower N state at point A and hence there must be a stationary kink between A and B. The position of the kink may be found by adding a curve corresponding to the set of temperatures that gives a stationary (zero-velocity) N kink between the upper and lower N states at each intensity. This curve has been added to Fig. 11. The position of the kink corresponds to the intersection of the zero-velocity curve and the beam curve (at point Z). Any kink to the left or right of Z will move quickly to the point of intersection.

Having introduced the I-T representation we can now apply this to consider the details of whole-beam oscillations.

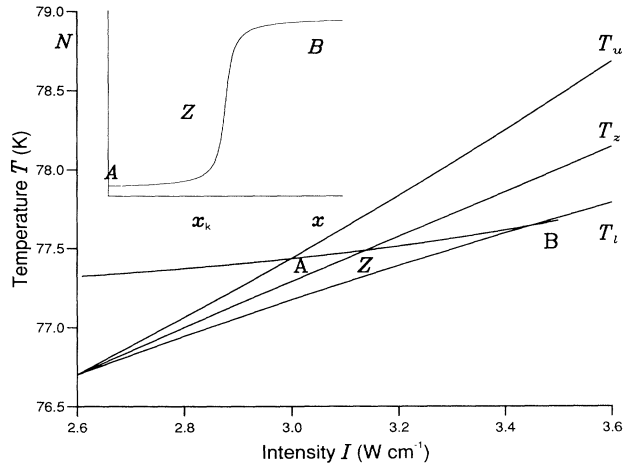

FIG. 11. An example where the beam is switched on where it descends below T_l and is off outside the bistable region where the temperature is low. The position of the kink is given by the intersection of the beam curve and the zero-velocity curve at Z.

1. *Whole-beam oscillations*

Results from numerical simulation of whole-beam oscillations were shown in Figs. 6–7. We now reconsider this process in the framework of the I-T representation. The coupled system is simulated numerically for a wide Gaussian input beam of spot size $w = 60 l_N$. The solution evolves from the homogeneous initial condition $N = 0$ and $T = 77$ K at $t = 0$. Once the oscillations have settled down we choose various points in time and reconstruct the beam curves from the $T(x)$ and $I(x)$ profiles. The parameters used are given in the caption for Fig. 6.

At $t = t_a$ all points on the beam are in the lower N state. In the I-T plane the beam curve corresponds to the curve labeled 1 in Fig. 12(a), where t is somewhat less than t_a. (Note that in this instance the beam curve in fact represents both sides of the temperature profile because of the symmetry in the solution about the center of the Gaussian beam.) At this moment the temperature is slowly decreasing and hence the beam curve moves downwards. A critical moment occurs when the beam curve (curve 2) cuts the curve bounding the bistable region. At this moment the only possible state in the center of the beam ($I = I_0$) is the high-N state. Hence the carrier profile switches up in the center. Kinks rapidly develop and move outwards. The velocity of the kinks depends on local irradiance and temperature. (This process occurs on the N time scale and hence we may neglect any temporal change in temperature while the kinks are in motion.) Both kinks stop at point Z, where $I = I_z = I(x_z)$ fixes the position of the kink. Once the high-N state appears the extra heat source (carrier recombination) causes an increase in temperature. This heating occurs mainly in the center of the beam (to the right of point Z), although heat is of course spread by diffusion. Hence the beam curve moves upwards, increasing more rapidly to the right of Z. This gives rise to the set of curves 3,4,5,... in Fig. 12(b). The interface between N states (at Z) moves to higher intensities and subsequently the switched-up region is contracting on the thermal time scale. When a portion of the beam curve crosses the zero-velocity curve the upper-N state collapses [Fig. 12(c)]. Alternatively, for very wide beams the kinks intersect at point B corresponding to the center of the beam. This collision appears to result in the collapse of the upper state. (Note that there are other possibilities if the beam is not Gaussian.) After collapse the system cools due to the drop in carrier recombination. Eventually the temperature drops to a level where the process repeats again.

In Fig. 13 we show a range of beam curves during the oscillation, showing how the oscillation is indeed bounded by the bistable region and zero-velocity curves. The switch-on does indeed occur at point A and similarly the switch-off when there is no longer a point of intersection with the zero-velocity line. The point Z also accurately gives the position of the edges of the switched-up region following initial expansion. Note that it is possible for the beam curve to fall below A since thermal diffusion may prevent an immediate temperature rise as the upper-N state appears.

The above considerations of the numerically obtained

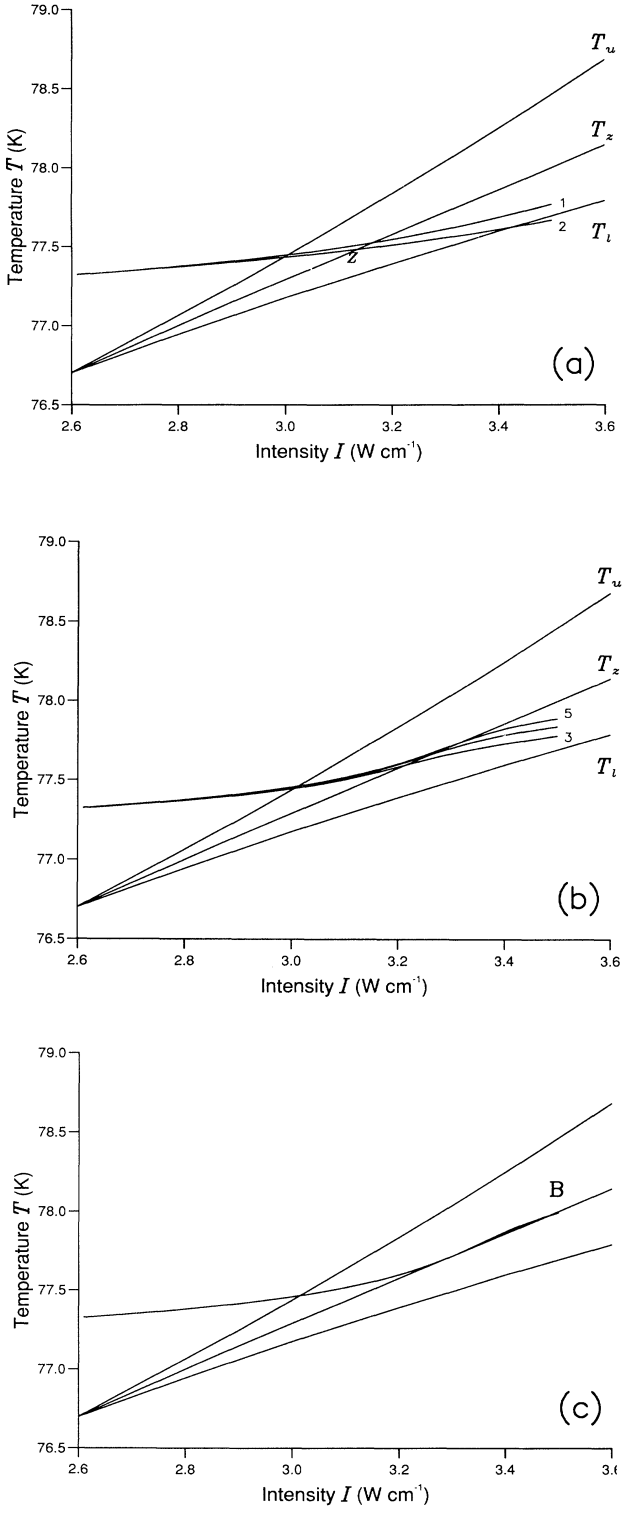

FIG. 12. Beam curve movement during oscillations: (a) The temperature is decreasing here and the beam curve moves downwards. When position (2) is reached, the center of the beam switches up since only the upper N state is accessible. (b) The temperature is increasing and the beam curve rises. (c) In this example the beam curve crosses the zero-velocity curve and the upper state collapses.

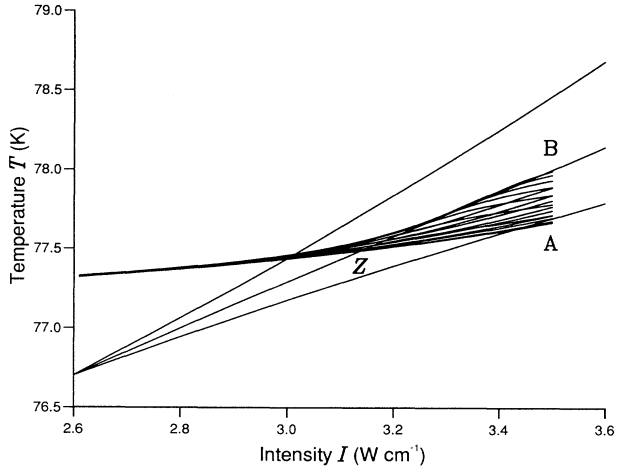

FIG. 13. An example of a set of beam curves during a whole-beam oscillation.

solution illustrate how the I-T representation can be used to describe whole-beam oscillation. The proposed technique allows the determination of the parameters where the high-N state appears and collapses, and an explanation of the transverse switching dynamics. Furthermore, as we will explain, plotting the steady beam curve in the I-T plane we can determine how to change the parameters to obtain oscillations.

For example, consider the isocline and I-T curves shown in Figs. 14(a) and 14(b), where the solution is stable and the carrier profile is switched up in the center. The incident beam is Gaussian with $w = 22l_N$. First note that the isocline representation does not predict oscillations. We can see from the I-T curves that the temperature must be increased to facilitate the switch-off. In general it is very difficult to see how the parameters could be changed to achieve this. Merely increasing the incident irradiance may not help; the beam curve would be extended to the right and an even higher temperature rise would be required. We will choose one parameter (the spot size) and change this to see what happens. Direct prediction of the result is not possible due to the complexity of the system and the disparate diffusion lengths. However, we may perform the simulation again with the altered parameter and see how the steady beam curve alters. Increasing the spot size to $w = 45l_N$ yields Figs. 14(c) and 14(d). Now the temperature is almost high enough, and only a small change is needed to induce the switch-off. If the spot size is increased further, then oscillations are obtained. It is possible that a change would yield a switched-off steady state rather than an oscillatory one. In that case the same process may be used to find parameters to give the switch-on and therefore continuous oscillations. We could have chosen any parameter and used the same procedure. The isoclines' representation is unhelpful in this case since they change with intensity and do not directly yield the switch points.

We have checked the validity of the I-T description in

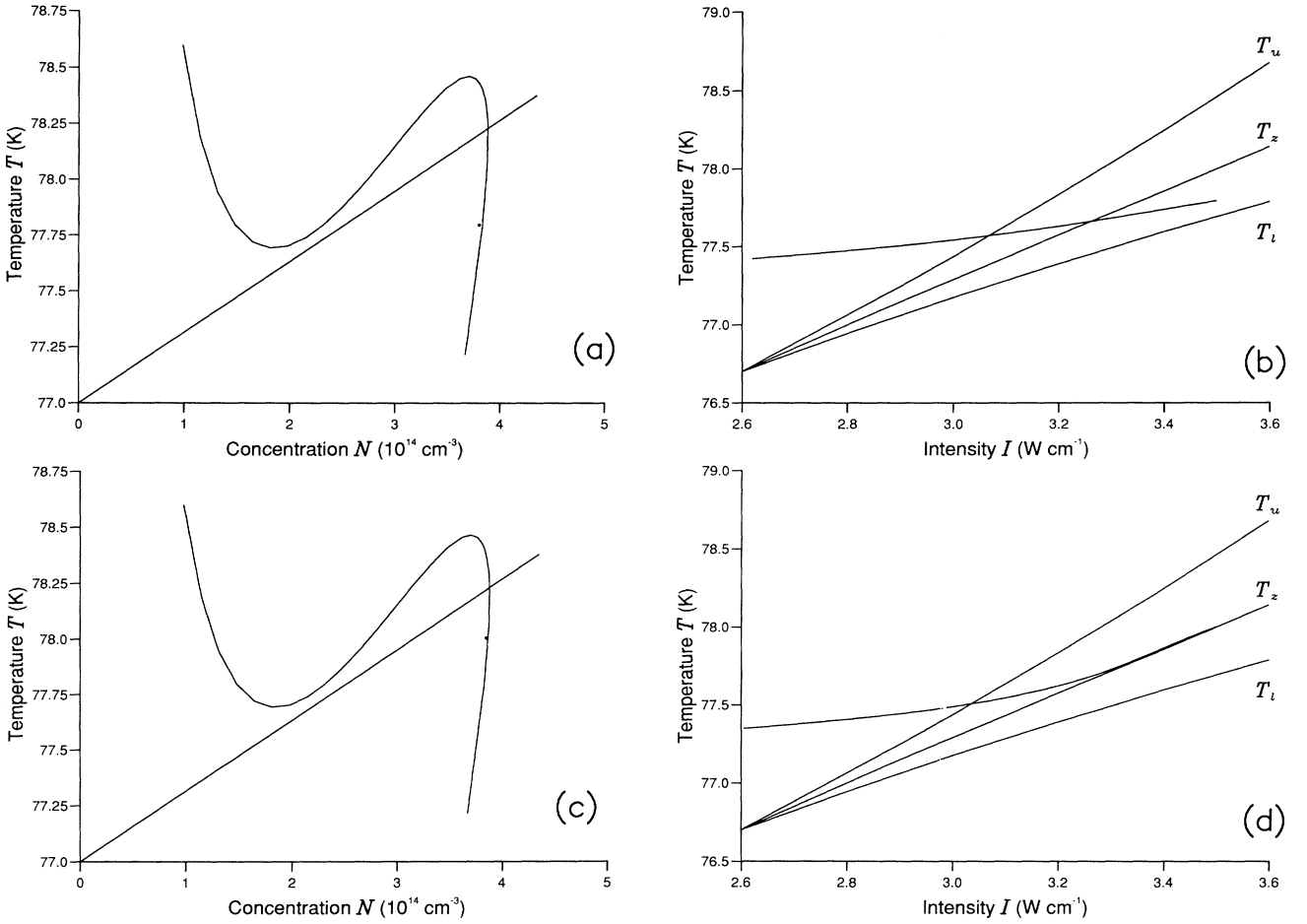

FIG. 14. (a) Center of beam superimposed on isoclines. (b) I-T representation corresponding to (a). For (c) and (d) the parameters are the same except for a larger spot size.

the limit when the carrier diffusion length is much less than the characteristic thermal diffusion length and the spot size. It is worth noting that as the spot size (or the thermal length l_T) decreases, the approximation of infinitely narrow kink widths will break down. In this limit the I-T technique fails to yield an adequate quantitative description of the oscillations. For example, it does not predict the correct position of the kinks. Nevertheless, the qualitative behavior remains the same.

The system can be modeled by solving the thermal diffusion equation and defining the carrier density from the method above. This would be very fast compared to solving the complete system and only loses information about the (fast) switch-on process.

2. *Single-shot regime*

The I-T allows the prediction of suitable conditions for the appearance of the "single-shot" regime for the Gaussian beam. This was possibly observed experimentally by Grigor'yants [1] following an earlier consideration in the plane-wave limit [19]. In this regime a small tran-

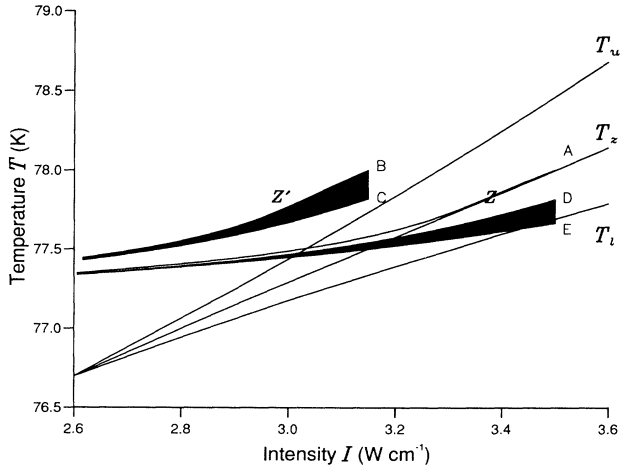

FIG. 15. Single-shot response. From the initial position (A) a drop in intensity produces B–C. Restoration of intensity yields position D and cooling eventually leads to a switch-on at E.

sient pulse (or drop) in intensity may yield a large output pulse, typically of much greater duration. In Fig. 15 the initial profile (A) has a central switched-up region with kinks at Z. A reduction in intensity moves all points on the beam curve to lower intensities (curve B), which is completely above the zero-velocity line. The upper state must collapse and this happens on the carrier time scale. Following collapse the system cools and the beam curves move downwards: $B \rightarrow C$. When the intensity is restored the beam curve switches to D while still cooling towards E, where once T_l is reached, the upper state will appear. The pulse duration may be quite short since the switch-off is very rapid. A similar process occurs for a sudden increase in irradiance.

3. Edge oscillations

The numerical simulations have revealed that the edges of the switched-on region (corresponding to the high-N state) may lose their stability and start to oscillate. The frequency of these oscillations is much higher than that of the whole-beam oscillations described in the previous sections. When the whole-beam oscillations also exist, the pulsations of the edges develop soon after the appearance of the upper state, their amplitude increases and they disappear with the collapse of the upper state (Fig. 16).

In cases when the whole-beam oscillation does not occur we have observed both symmetric and antisymmetric pulsations of the edges. An example of edge oscillations with no associated whole-beam oscillations is given in Fig. 17(a). We defer for a planned forthcoming publication a more extensive examination of the edge oscillations. We will, however, note that this phenomenon corresponds to almost tangential orientations of the beam curve to the zero-velocity curve in the I-T representation [Fig. 17(b)]. Hence the position of the kinks is very sensitive to the temperature. Note that the beam curve does not quite intersect the zero-velocity curve; this is probably due to our assumptions of infinitesimally small kink width.

It could be that both whole-beam and edge oscillations are manifestations of layer oscillations [16] under the constraints of the inhomogeneous input profile. The possibility of high-frequency edge oscillations in this system is intriguing since this may explain similar oscillations observed experimentally [1], where the frequency was much higher than would be expected from the thermal time.

C. Numerical method

The large ratio of the reaction rates in the coupled equations classifies the system as a stiff set of equations. For efficient numerical integration this stiffness required using an implicit integration scheme. In particular, we used the backward differentiation formulas of Gear [20] with variable order and variable time-step control.

We approximated the spatial derivatives using finite differences on a uniform mesh with Neumann- or no-

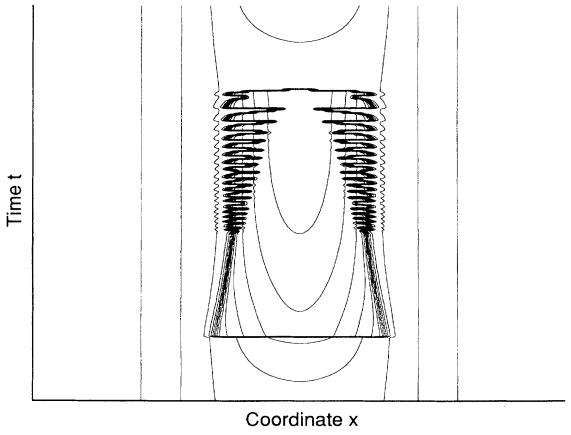

FIG. 16. Contour plot of carrier concentration evolving in time as a function of x. The central portion switches up and the edges lose stability producing oscillations.

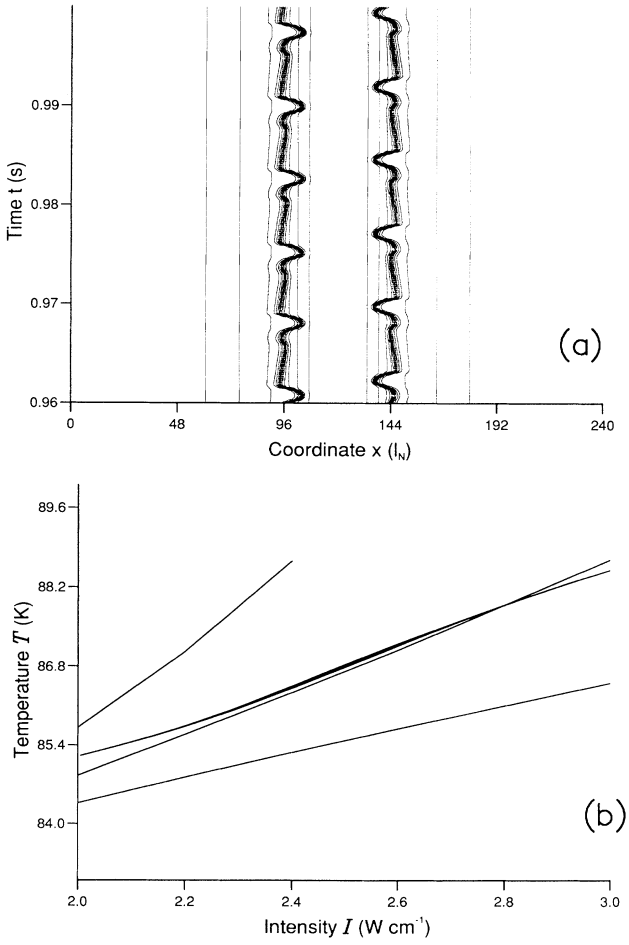

FIG. 17. (a) Contour plot of carrier concentration evolving in time as a function of x. There are only edge oscillations and no whole-beam oscillations. (b) I-T representation for the edge oscillations showing that the beam curve is almost tangential to the zero-velocity curve.

flux-type boundary conditions. When using an implicit method a system of nonlinear algebraic equations must be solved at each step. The nature of this differencing scheme leads to a banded algebraic system with the band width determined by the order of the approximation to the derivatives. On each time step we solved the system using Newton's method with a banded matrix solver.

It was quite possible to use this method with our available computer power (Meiko i860 computing surface). However, a two-dimensional code will be on the verge of practicability.

IV. CONCLUSIONS

We have theoretically and numerically investigated oscillations in an InSb bistable étalon with competing nonlinearities. We have developed a method that explains many features of the oscillations, in particular the propagation of kink solutions. This relies on the stiff nature of the InSb system, where the time constants are radically different and the fast subsystem diffuses to a lesser extent than the slow subsystem. The method is useful when attempting to find parameter ranges that yield oscillations. The full system has been solved numerically in one transverse dimension and the properties of kink solutions, whole-beam and edge oscillations investigated. The numerical simulations confirm the theoretical approach. For small spot sizes (of the order of the carrier diffusion length), kink solutions are no longer applicable and the numerical approach has to be used exclusively. The oscillations must be similar in two transverse dimensions and two-dimensional simulations are underway to confirm this. We have shown that layer oscillations are possible even in this highly inhomogeneous system. Because we are limited to one transverse dimension we do not attempt quantitative agreement with experiment. Qualitatively there is good agreement. We are able to explain the high-frequency oscillations observed experimentally as either edge oscillations or a very small thermal decay time.

ACKNOWLEDGMENTS

This work was supported by the SERC Computational Science Initiative (Grant No. GR/G 13044). One of the authors (Yu.R) gratefully acknowledges support from the Royal Society, London.

[1] A. V. Grigor'yants and I. N. Dyuzhikov (unpublished).
[2] A. V. Grigor'yants, Yu. A. Rzhanov, and Yu. I. Balkarei, Kvant. Elektron (Moscow) **14**, 128 (1987) [Sov. J. Quantum. Electron. **17**(1), 72 (1987)].
[3] H. Richardson and Yu. A. Rzhanov (unpublished).
[4] H. S. Carslaw and J. C. Jaeger, *Conduction of Heat in Solids*, 2nd ed. (Oxford University Press, New York, 1959).
[5] W. J. Firth and I. Galbraith, J. Mod. Opt. **34**, 137 (1987).
[6] D. Frank. Opt. Commun. **62**, 61 (1987).
[7] P. C. Fife, *Mathematical Aspects of Reacting and Diffusing Systems* (Springer-Verlag, Berlin, 1970).
[8] R. H. Harding and J. Ross, J. Chem. Phys. **92**, 1936 (1990).
[9] A. A. Andronow and C. E. Chaikin, *Theory of Oscillations* (Princeton University Press, Princeton, 1949).
[10] S. L. McCall, Appl. Phys. Lett. **32**, 284 (1978).
[11] E. Abraham, Opt. Commun. **61**, 282 (1986).
[12] J. L. Jewell, H. M. Gibbs, S. S. Tarng, A. C. Gossard, and W. Weigmann, Appl. Phys. Lett. **40**, 291 (1982).
[13] Yu. D. Kalafati and Yu. A. Rzhanov, in *Nonlinear Waves 1—Dynamics and Evolution*, edited by A. V. Gaponov-Grekhov, M. I. Rabinovich, and J. Engelbrecht, Research Reports in Physics (Springer-Verlag, Berlin, 1987), pp. 159–167.
[14] H. Ikeda, M. Mimura, and Y. Nishiura, Nonl. Anal. TMA. **13**, 507 (1989).
[15] Y. Nishiura and M. Mimura, SIAM J. Appl. Math. **49**, 481 (1989).
[16] S. Koga and Y. Kuramoto, Progr. Theor. Phys. **63**, 106 (1980).
[17] Yu. D. Kalafati, I. A. Serbinov, and L. A. Ryabova, Doklady Akad. Nauk SSSR **263**, 862 (1982) [Sov. Phys. Doklady **27**, 310 (1982)].
[18] H. A. MacKenzie, J. J. E. Reid, H. A. Al-Attar, and E. Abraham, Opt. Commun. **60**, 181 (1986).
[19] A. V. Grigor'yants, Yu. A. Rzhanov, M. I. Elinson, and Yu. I. Balkarei, Kvant. Elektron (Moscow) **14**, 2047 (1987) [Sov. J. Quantum. Electron. **17**, 1306 (1987)].
[20] C. W. Gear, *Numerical Initial Value Problems in Ordinary Differential Equations* (Prentice Hall, Englewood Cliffs, NJ, 1971).